IAC-14,C1,2,13

COUPLED ORBIT-ATTITUDE DYNAMICS OF A CAPTURED ASTEROID DURING SWING-BYS

D. García Yárnoz,
Advanced Space Concepts Laboratory, University of Strathclyde, Glasgow, UK, Daniel.Garcia-Yarnoz@strath.ac.uk

C. R. McInnes
Advanced Space Concepts Laboratory, University of Strathclyde, Glasgow, UK, Colin.McInnes@strath.ac.uk

The rotational state and structure of minor bodies undergo major disruptions during very close encounters with massive bodies. This paper proposes the use of tidal interaction during a swing-by to modify or manipulate the spin and possibly the structure of asteroids, primarily during capture. The possibility of de-spinning, spinning-up or controlled break-up of a captured asteroid is considered. Three simple planar models are used to study the orbit-attitude interactions: the coupled dynamics of an ideal mass-point dumbbell, a simplified decoupled rigid body rotation dynamics, and a circular orbit binary. The evolution of the rotational state and structure of the asteroids is studied for the hypothetical cases of a single lunar or Earth swing-by prior to capture. The final conditions are shown to be highly dependent on the initial rotational state, the distance to the swing-by body, and, most importantly, the relative attitude of the asteroid to the local vertical at pericentre.

I. INTRODUCTION

Recent interest in the capture of asteroids for scientific purposes or exploitation has generated a series of proposals for asteroid retrieval missions to various target orbits. A number of these proposals utilise swing-bys of the Moon or Earth to reduce the asteroid hyperbolic excess velocity and the associated insertion burns into the final capture orbit.

NASA's Asteroid Retrieval Mission, loosely based in the Keck's study report [3], foresees using a lunar swing-by to reduce the capture energy into a lunar Distant Retrograde Orbit as the final destination for the retrieved asteroid. Strange et al. [16] study capturable asteroids with this strategy, imposing a lunar swing-by height constraint as low as 50 km above the lunar surface. Following a slightly different approach, Sanchez Cuartielles et al. [11] suggest the use of multiple Earth passes (at large distances) to reduce the long-term capture costs of small asteroids. Although they consider only weak interactions far from what we normally refer to as a swing-by, the possibility of using high altitude Earth gravity assist may reduce even further the required energy for capture. More relevantly, the extended lifetime trajectories of Temporarily Captured Orbiters (TCO) proposed by Urrutxua et al. [18] do comprise much closer Earth passes in their weakly captured trajectories.

Given the large mass and inertia of asteroids, and the usually irregular shape of the smallest bodies in the NEO family, which represent the best candidates for capture or TCO lifetime extension with current technology, a close swing-by of a massive body, be it the Earth or the Moon, will induce large variations in the rotational state and possibly the structure of the asteroid. These interactions may pose serious challenges for the attitude control of asteroids during capture. Whether they are bagged, attached to a spacecraft or not, large quantities of fuel may be required to counteract the torque build-up. On the other hand, if engineered, the disruption events can be seen as opportunities to modify the spin or structure of the asteroid at zero or low costs. This paper proposes the utilisation of the tidal induced torques during a swing-by for rotational state manipulation, separation of contacts binaries or even (partial) disintegration of rubble piles.

To this end, the effect of the coupling between attitude and orbit dynamics for this particular case has been studied with a series of simple planar models. They provide insight into the rotational state upheaval and the chance of break-up of the asteroid during the close approach. Three different dynamic models (and a combination of two of them) are considered:

1. A dumbbell of two equal point-masses connected with a massless rod to demonstrate coupled orbit-attitude dynamics during close passes

2. A simplified rigid body (of various shapes) in which the attitude and rotation evolution is decoupled from the orbit propagation

3. A binary pair with two small asteroids with common gravitational attraction and initially rotating around their barycentre

4. An equal mass contact binary (model 2) with the possibility of separation as the rotation rate increases into a binary pair (model 3)

In order to observe the dependence with the swing-by conditions, the well known asteroids 2004 MN4 (also known as Apophis) and 2006 RH120 are selected as the test cases for these three simple models. The hyperbolic excess velocity for the swing-bys is thus selected as that of their close approaches to Earth on years 2029 and 2028 respectively. Their size, shape, rotational state and structure are however modified to match the assumptions of the different models.

II. ROTATION AND STRUCTURE DISRUPTION OF ASTEROIDS DURING PLANETARY SWING-BYS

The evolution and changes of rotation rate of minor bodies can be explained through YORP effect, encounters with planets or larger bodies, and possibly also collisions [10]. Comets have in addition spin changes due to outgassing. Due to larger time scales for the YORP effect, fast or abrupt alterations of the rotational state are mainly caused by a swing-by of a major body of the solar system. They may induce tumbling and place them in complex rotational states, and they can also cause a disruption of their structure through tidal torques.

One of the earliest results related to tidal disruption is the Roche limit [4], defined as the distance below which forces will disintegrate an orbiting object held together only by self-gravity. Since the original definition for a fluid satellite in 1848 by Roche, there has been numerous definitions of such a tidal break-up limit for various types of internal strength, rigidity and material properties. Davidsson [5, 6] provides a good overview of previous analysis and calculates varying Roche limits for rotating asteroids with internal strength, showing that for very small asteroids the Roche limit decreases considerably.

However, Roche limits normally refer to orbiting satellites. For a single swing-by event, it provides an initial estimate of the distances below which tidal disruption is significant, but the outcome of a swing-by depends on the particular geometry of the encounter and the structure and characteristics of the body. The effect on the rotation state of the asteroid can also be felt at much greater distances than the Roche limit. Scheeres et al. [14] show that swing-bys radically affect the spin state of asteroids and can induce asteroids that previously had uniform rotation into a tumbling state. Richardson et al. [9] demonstrate with a multi-particle model with self-gravity that for low-velocity encounters at distances less than 3 Earth radii the structure of a rubble pile can be completely distorted. This may lead to the formation of very elongated bodies, double-lobed asteroids or contact binaries. Similar processes may explain crater chains in the Moon and other solar system bodies.

Doublet and multiple crater impacts have also been explained by binary asteroids generated by previous encounters with Earth, or possibly also a break-up during the approach [17]. Farinella and Chauvineau [8] studied such close encounters of binaries with Earth, first with a linear approximation, and late with a more general hyperbolic trajectory. They conclude that disruptions during these encounters may explain doublet craters, the formation of contact binaries as one stable outcome, as well as slow rotators or binaries with wide distances between the components of the pair. Energy dissipation may play an important role to achieve stable configurations after the disruption caused by a swing-by. Fang and Margot [7] argues that these close encounters can increase or decrease the semi-major axis of a binary and break tidal locks, and they may also affect BYORP, shutting it down.

All these effects can be explained by the coupling of the attitude and orbit of non-symmetric bodies. It is also the cause of tidally locked satellites, and can be used for attitude control by gravity gradient. Sincarsin and Hughes [15] studied this coupling for very large spacecraft, and their conclusions are partly applicable to asteroids, if we do not consider deformations or restructuring. In the frame of an asteroid capture mission, they will need to be taken into account, to avoid undesired rotation rate changes or break-up, or to be used instead to control the rotation rate or cause an intended break-up.

III. DYNAMICAL MODELS

This section presents the dynamical models employed in the paper, and the test cases used to validate them. All models presented are planar, with the rotational axis of the asteroid or binary pair perpendicular to the orbital plane. This is a considerable simplifying assumption, as it avoids any instance of tumbling, complex rotation or off-plane forces. However, the tidal torques experienced by the asteroid or the binary are greatest in the planar case. It thus still represents a limiting case of interest where the stronger tidal torques will cause larger variations in the rotation state.

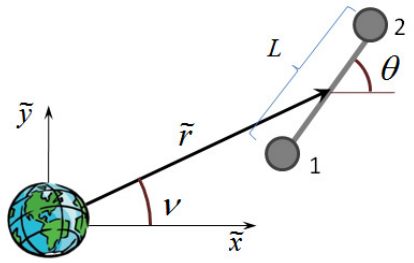

Figure 1: Schematic of the dumbbell planar problem definition.

III.I Coupled dynamics of point-mass dumbbell

The simplest of models to study the coupled dynamics of a non-spherical satellite around a spherical massive body is an ideal equal mass dumbbell, assuming point-masses linked with a massless rod of given length L. The dumbbell rotates along an axis of maximum moment of inertia, and this axis is assumed perpendicular to the orbital motion. The coupled orbit-attitude equations of motion for the planar case of such a dumbbell (modified from [2] removing the solar radiation pressure and normalizing), are given by:

$$\begin{aligned}
\ddot{r}-r\dot{\nu}^2+\frac{\frac{\mu}{2}\left(r-\frac{1}{2}\cos(\theta-\nu)\right)}{\left[r^2-r\cos(\theta-\nu)+\frac{1}{4}\right]^{\frac{3}{2}}}+\frac{\frac{\mu}{2}\left(r+\frac{1}{2}\cos(\theta-\nu)\right)}{\left[r^2+r\cos(\theta-\nu)+\frac{1}{4}\right]^{\frac{3}{2}}}&=0\\
\dot{\nu}+\frac{2\dot{r}\dot{\nu}}{r}+\frac{\frac{\mu}{4r}\sin(\theta-\nu)}{\left[r^2+r\cos(\theta-\nu)+\frac{1}{4}\right]^{\frac{3}{2}}}+\frac{\frac{\mu}{4r}\sin(\theta-\nu)}{\left[r^2-r\cos(\theta-\nu)+\frac{1}{4}\right]^{\frac{3}{2}}}&=0\\
\ddot{\theta}+\frac{\mu r\sin(\theta-\nu)}{\left[r^2-r\cos(\theta-\nu)+\frac{1}{4}\right]^{\frac{3}{2}}}+\frac{\mu r\sin(\theta-\nu)}{\left[r^2+r\cos(\theta-\nu)+\frac{1}{4}\right]^{\frac{3}{2}}}&=0
\end{aligned} \tag{1}$$

where r is the distance from the massive body to the centre of mass of the dumbbell, ν is the true anomaly or an equivalent angle between the position vector of the dumbbell and a reference direction in an inertial frame, and θ is the angle the dumbbell forms with the same reference direction. All distances have been normalised by the length of the dumbbell L , and thus $r = \tilde{r}/L$ and the mass parameter $\mu = \tilde{\mu}/L^3$, where tilde variables represent fully dimensional variables. Figure 1 shows an schematic of the dumbbell and the state vector variables definition for this particular problem.

The equations can be therefore rewritten as:

$$\begin{aligned}
\ddot{r} - r\dot{\nu}^2 + \frac{\mu}{2}\frac{r_1}{{d_1}^3} + \frac{\mu}{2}\frac{r_2}{{d_2}^3} &= 0\\
\ddot{\nu} + 2\frac{\dot{r}\dot{\nu}}{r} + \frac{\mu}{4r}\sin(\theta-\nu)\left(\frac{1}{{d_2}^3} - \frac{1}{{d_1}^3}\right) &= 0\\
\ddot{\theta} + \mu r\sin(\theta-\nu)\left(\frac{1}{{d_1}^3} - \frac{1}{{d_2}^3}\right) &= 0
\end{aligned} \tag{2}$$

in which r_1 and r_2 are given by:

$$r_1 = r - \frac{1}{2}\cos(\theta-\nu); r_2 = r + \frac{1}{2}\cos(\theta-\nu) \tag{3}$$

and d_i is:

$$d_i|_{i=1,2} = {r_i}^2 + \frac{1}{4}\sin^2(\theta-\nu) \tag{4}$$

The three coordinates r, ν and θ are all interdependent, and rotational energy can be transferred to orbital energy and vice-versa, as shown in [2]. The different accelerations are a function of the angular difference $\theta-\nu$, which is the angle between the dumbbell and the local vertical. The term prograde rotators will be used throughout the paper for bodies rotating in the same direction as the orbital motion ($\dot{\theta} > 0$). They are more susceptible to tidal torque disturbances than retrograde rotators, as they more likely to enter into resonance with the orbit motion.

As a particular example, we select a test case of an asteroid composed of 2 constant density spheres of 50 m radius, separated just 100 m (so in essence a solid double sphere contact binary, but modelled as a point-mass dumbbell). This captured asteroid is assumed to be located on a very high eccentricity orbit with an apocentre radius equal to the mean lunar distance from the Earth, and a pericentre radius of the order of 2 Earth radii. This is a relevant case if a lunar swing-by followed by an Earth close passage is to be used as the first step to capture an object in an Earth bound orbit. The final rotation rate at the next apocentre at the quasi-Moon distance is shown in Fig. 2 for various initial rotation rates $\dot{\theta}_0$ as a function of $\theta - \nu$ at pericentre. Initial prograde rotation rates are plotted with solid lines, while retrograde rotation rates are dashed.

Three horizontal lines mark rotation rates of note. The highest is the spin rate at which a rotating sphere (with no internal strength or other cohesive forces between particles) would start shedding mass at its equator. It is given by:

$$\dot{\theta}_{shed} = 2\sqrt{\pi G\rho/3} \tag{5}$$

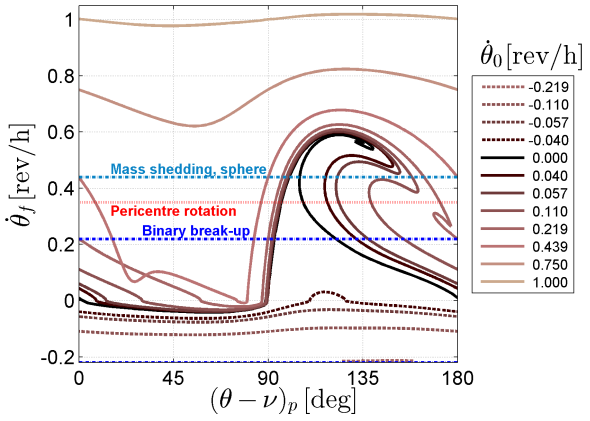

Figure 2: Final rotation rate for a point-mass dumbbell as a function of the angle with the local vertical at pericentre.

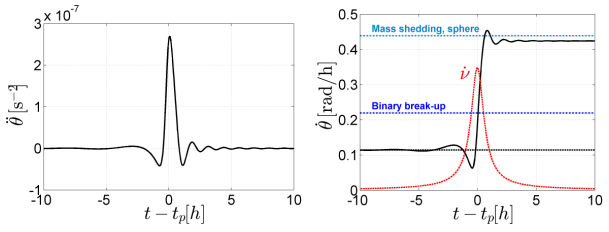

Figure 3: Instantaneous angular acceleration and rotational speed evolution due to tidal torque for a point-mass dumbbell in a highly elliptical orbit with pericentre at 2 Earth radii.

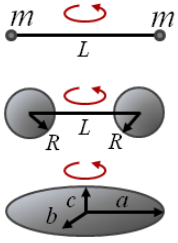

$$I^* = \frac{I_{yy}-I_{xx}}{I_{zz}} = 1$$

$$I^* = \frac{5}{8(R/L)^2+5}$$

$$I^* = \frac{1-(b/a)^2}{1+(b/a)^2}$$

Figure 4: Various rigid body configurations and their associated moments of inertia ratios

and it is only a function of the density of the orbiting body ρ, with G being the gravitational constant. This shedding limit, also known as rubble pile spin barrier, is plotted on the previous figure for the case of an average density of 2.1 g/cm^3, which corresponds roughly to a period of 2.3 hours. For large rubble pile asteroids, it represents a maximum spin rate before they start shedding mass, while for smaller ones, higher spin rates have been observed, which can be explained either by a monolithic structure or by cohesive forces that bind them together and hinder the mass shedding [12, 13]. An additional useful limit is the rotational speed at which an equal mass double-sphere contact binary would split if no internal forces or cohesion are considered. This rotational speed is exactly half the mass shedding limit (period of approximately 4.6 hours). For contact binaries of different size the break-up speed without cohesion would lie between the former two. The third intermediate line is the maximum true anomaly variation for the orbit, which always takes place at the pericentre.

It can be observed in Fig. 2 that the spin of fast prograde rotators (of more than one revolution per hour) and retrograde rotators is not strongly affected by the tidal torques during a pericentre passage. Slow prograde rotators and non-rotating dumbbells can however be effectively de-spun, or spun up above the binary break-up or mass shedding limit depending on the configuration at pericentre. The spin rates acquired can be higher that the rotation rate at pericentre $\dot{\nu}_p$. In general, the dumbbell is spun up when $\theta - \nu$ is the range $90 - 180°$ (positive torque at pericentre), and de-spun for angles in the range $0 - 90°$.

A low spin rate at the end of the propagation does not discard the possibility that any of these limits was surpassed during the pericentre passage. Fig. 3 presents the evolution of the torque acceleration and the rotational state for a particular case with an initial rotation period of 5.8 hours. As expected, most of the interaction takes place at pericentre in a bracket of 4 hours around the closest approach. Due to the configuration at the pericentre with a $\theta - \nu$ angle of 165°, the net result is an acceleration in the rotation of the dumbbell. Even though the final spin state is below the mass shedding limit, this is surpassed right after pericentre and mass loss could have occurred.

III.II Decoupled dynamics of a rigid body

The coupling between attitude and orbit in the case of the dumbbell shown above (or any other rigid body) is weak [15], with only small perturbations to the in-plane orbital elements. The predominant effect is thus changes in the rotational state. As such, the system of equations can be considered decoupled for characteristics lengths of the body much smaller than the orbital radius. Then, the asteroid can be modelled as a rigid body rotating around the axis of largest moment of inertia (minimum energy configuration), which is assumed perpendicular to the orbital plane. As in the previous dumbbell case, deformations or any type of reconfiguration are ignored.

In addition to solving the traditional decoupled orbital equations of motion for the centre-of-mass of the rigid body, the attitude of the asteroid is propagated by integrating the equation for the torque acceleration, which can be expressed by (adapted from [1]):

$$\ddot{\theta} + \frac{3\mu}{2r^3}\frac{I_{yy} - I_{xx}}{I_{zz}}\sin 2(\theta - \nu) = 0 \qquad (6)$$

where $I_{zz} > I_{yy} > I_{xx}$ are the principal moments of inertia of the body. This differential equation depends only of a "shape" parameter I^* given by the ratio of the body's moments of inertia, and is independent of the size of the object. For several simple shapes I^* can be calculated with the expressions given in Fig. 4. The extreme case of an ideal "point-mass" dumbbell has a value of 1 (very elongated object), while a spherical body would result in a shape factor of zero.

Figure 5 plots the final spin state of a rigid body after a test case equivalent to a close encounter at 2 Earth radii as described in the previous section. The "point-mass" dumbbell shape reproduces almost exactly the results of the coupled orbit-attitude dumbbell equations. For less elongated shapes, the smaller shape factor reduces the

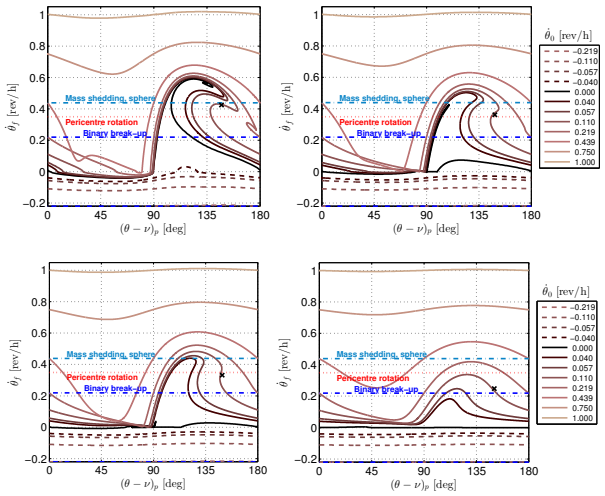

Figure 5: Final rotation rate for rigid solid with point-mass dumbbell shape (top-left, $I^* = 1$), equal spherical masses contact binary (assumed rigidly bound, top-right, $I^* \approx 0.71$), and two cases of tri-axial ellipsoids with $a = 2b$ and $a = \sqrt{2}b$ (bottom, $I^* = 0.6$ and $I^* \approx 0.33$ respectively)

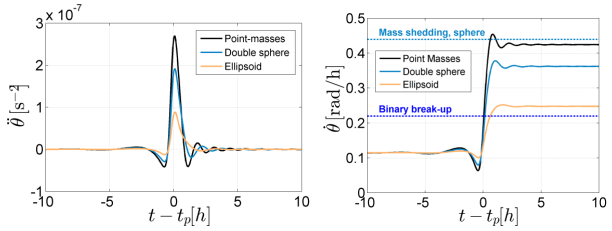

Figure 6: Comparison of the tidal torque acceleration and rotational speed evolution for three different rigid body shapes.

effect of the gravitational torque on the final rotational rate. Similar conclusions to section III.I can be drawn: fast prograde rotators and retrogade rotators are least affected.

Figure 6 compares a particular case (indicated with x markers in Fig. 5) with an initial rotation rate of half of the binary break-up spin limit for different rigid body shapes. The torque and its effects are considerably reduced for less elongated, more spherical bodies.

III.III Binary pair

Finally, we consider the case of a binary system performing a swing-by of a massive body, with the gravitational attraction between the two components of the binary modelled (the 1+N body problem with N=2).

The equations of motion for each of the two components of the binary pair are given by:

$$\ddot{\vec{r}}_i = -\mu \frac{\vec{r}_i}{{r_i}^3} - \frac{2}{3}\alpha\pi\rho G \frac{\vec{r}_i - \vec{r}_j}{|\vec{r}_i - \vec{r}_j|^3} \qquad (7)$$

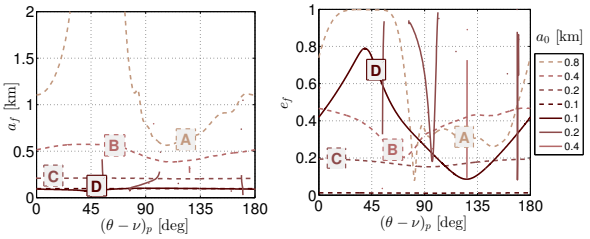

Figure 7: Final semi-major axis a and eccentricity e for an equal mass binary pair after a pericentre passage at 5 Earth radii.

where α_i is a function of the ratio of the radii of the binary pair:

$$\alpha = \frac{{R_1}^3 + {R_2}^3}{L^3} \qquad (8)$$

Distances are normalised with a reference length $L = R_1 + R_2$, where R_i are the radius of each of the elements of the binary, assumed spherical. For the case of an equal mass binary Eq. 7 results in:

$$\ddot{\vec{r}}_i = -\mu \frac{\vec{r}_i}{{r_i}^3} - \frac{1}{6}\pi\rho G \frac{\vec{r}_i - \vec{r}_j}{|\vec{r}_i - \vec{r}_j|^3} \qquad (9)$$

As a test case, an equal sized circular binary with a range of semi-major axes is assumed to perform a close encounter with Earth at pericentre distances of 2, 5 and 10 Earth radii. The components of the binary are assumed point masses, which implies that no impact is computed when the normalized distance between the binary centres is smaller than 1.

Figure 7 plots the semi-major axis and eccentricity of the binary system after a close encounter for the intermediate pericentre case (5 Earth radii). Similar plots have been generated for cases with both lower and higher pericentre radius. For the 2 Earth radii case, mostly retrograde rotating binaries with a small initial semi-major axis survive the close approach without a break-up and escape. There are a few single cases of geometrical configurations that allow prograde binaries to survive. For higher pericentres (for example the 5 Earth radii shown in Fig. 7) some prograde rotating binaries (solid lines) manage to maintain their binary structure and do not escape from each other. However, the initial semi-major axis is in most cases small (of the order of 100 m, case "D") and they suffer large variations in the binary orbit eccentricity. It can be observed in Fig. 7 that retrograde binaries fare better: for initial semi-major axes smaller than 400 m, the disruption introduced by the gravitational torque does not manage to break the binary pair. This limit increases to over 800 m for the case of a pericentre passage over 10 Earth radii.

Figure 8 shows the semi-major axis and eccentricity evolution, as well as a binary trajectory plot centred on

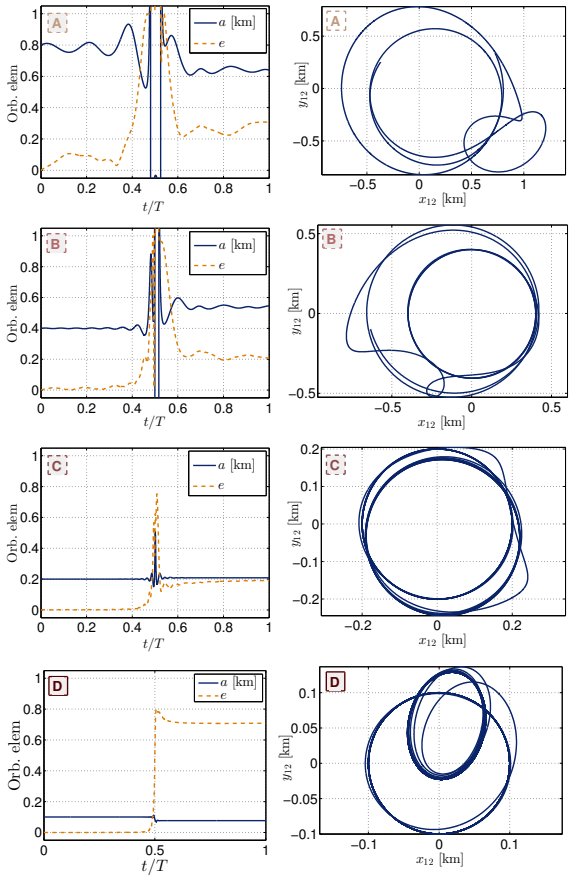

Figure 8: Binary semi-major axis a and eccentricity e evolution for an equal mass binary pair during a close approach (left), and trajectories of one of the components of the binary with respect to its companion. Initial trajectories are circular ($e = 0$).

one of the components of the pair, for 4 particular cases identified with letters in Fig. 7. Case "A" through "C" correspond to retrograde binaries of decreasing initial semi-major axis. It is clear that the disruption is smallest for the closest binary pair "C", with no apparent change in a and a small increase in eccentricity. In cases "A" and "B" the binary pair is technically broken at the pericentre passage (eccentricity larger than 1), but then gravitationally bound together in an elliptical orbit again when the gravitational torques reduce away from the closest approach. Case "D" represents one case of a surviving prograde close binary.

III.IV Equal mass contact binary

This model combines rigid body propagation and the binary pair model (see III.II and III.III), with switching events triggered by a limit rotational rate for break-up, and re-impact of the components.

For the rigid body propagation the shape factor of two spheres in contact is used. No sliding between boulders, independent boulder rotation, or other type of relative movement between the two components of the contact binary is considered. If the contact binary rotation speed reaches the binary break-up rotation limit, the pair splits and propagation continues with the binary pair model. This implies only self-gravity is considered, with no cohesion between the components of the contact binary. Reconfiguration of the binary takes place when the distance between the two components drops below two radii. No collision or reconfiguration due to the impact is computed.

IV. APPLICATION TO CAPTURE

In the event of an asteroid retrieval mission that requires a lunar swing-by (such as [3, 16]), or an Earth encounter at lower distances than those proposed in [11], the consequences of the swing-by on the minor body can be investigated with the above described models. In this section, both isolated single Earth and lunar swing-bys are considered, for different pericentre radii. No third body perturbation is included in the propagation of the trajectories. Two test cases have been run: a low velocity swing-by with infinite velocity $v_{inf} = 0.6479$ km/s, and a high velocity swing-by with $v_{inf} = 5.851$ km/s. They correspond to the hyperbolic excess velocities of the predicted encounters with Earth of asteroids 2006 RH120 and 2004 MN4 (Apophis) in years 2028 and 2029 (from JPL's Small–Body Database Browser[1]). Candidate asteroids for capture are more likely to have low v_{inf}, as asteroids with orbits close to that of the Earth will therefore have modest energy requirements for capture.

IV.I Isolated Earth Swing-by

Figures 9 and 10 plot the maximum rotation rate changes achievable with an Earth swing-by for the two swing-by velocities considered, as a function of their initial rotation rate. Positive variations correspond to the maximum achievable asteroid spin-up, while negative variations are the maximum de-spin. The pericentre radius ranges from two to ten Earth radii.

The dashed diagonal red line represents the mass shedding rotation limit: any point above this line corresponds to a rotation rate in which mass is being lost at the equator of the asteroid (assumed spherical) if no cohesion is taken into account. Similar lines can be plotted for the binary break-up limit (parallel to the mass shedding half the distance from the origin of coordinates) and for zero spin rate ($y = -x$, again parallel through the origin).

The plots on the right side have been normalised with respect to the rate of variation of the true anomaly at

[1] http://ssd.jpl.nasa.gov/sbdb.cgi Last accessed 20/06/2014

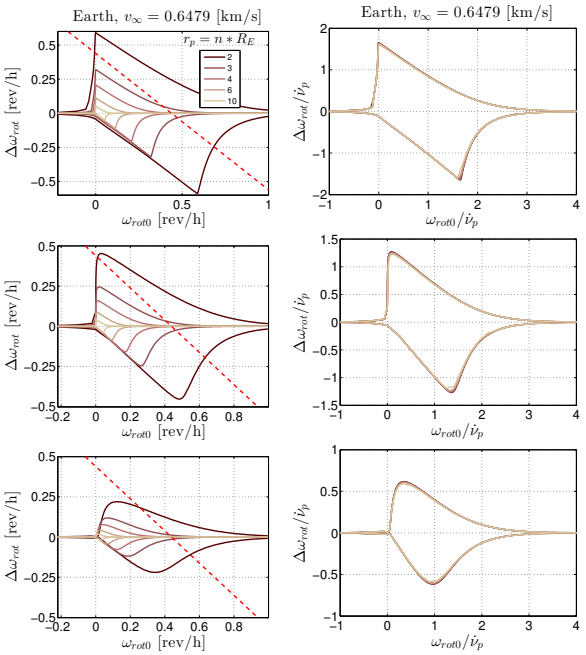

Figure 9: Maximum spin-up and de-spin achievable for a low-velocity Earth swing-by for various shape factors: point-mass dumbbell (top), equal mass contact binary (middle) and ellipsoid with $a = \sqrt{2}b$ (bottom). Right plots have been normalised with the true anomaly rate at pericentre $\dot{\nu}_p$.

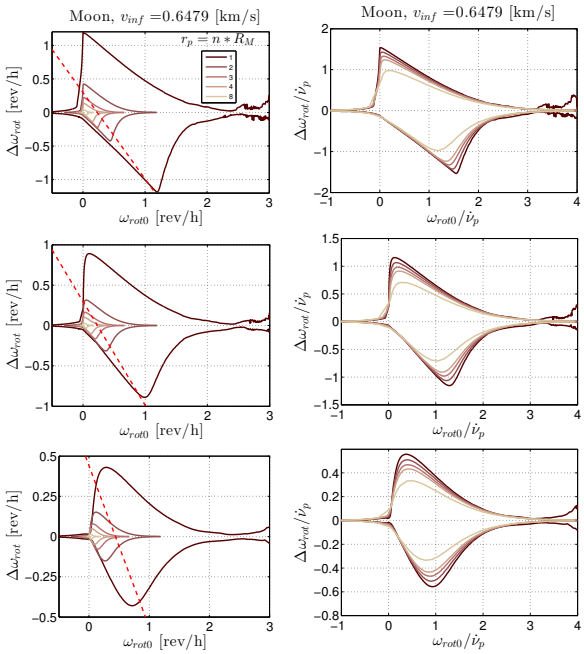

Figure 11: Maximum spin-up and de-spin achievable for a low-velocity Moon swing-by for various shape factors: point-mass dumbbell (top), equal mass contact binary (middle) and ellipsoid with $a = \sqrt{2}b$ (bottom). Right plots have been normalised with the true anomaly rate at pericentre $\dot{\nu}_p$.

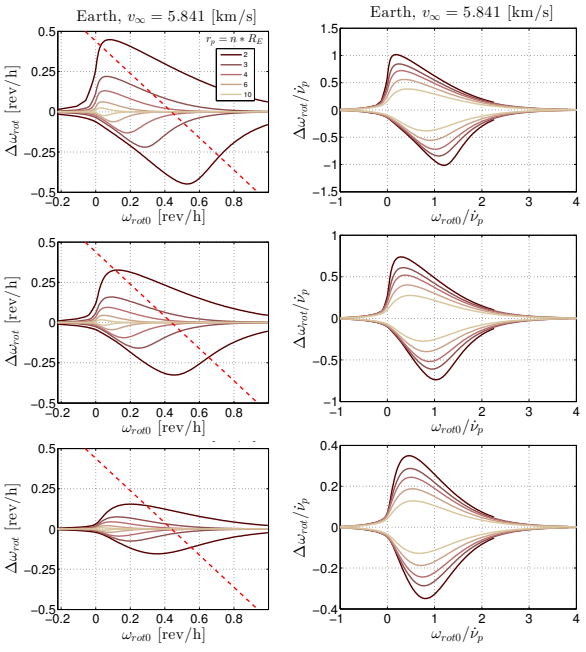

Figure 10: Maximum spin-up and de-spin achievable for a high-velocity Earth swing-by for various shape factors: point-mass dumbbell (top), equal mass contact binary (middle) and ellipsoid with $a = \sqrt{2}b$ (bottom). Right plots have been normalised with the true anomaly rate at pericentre $\dot{\nu}_p$.

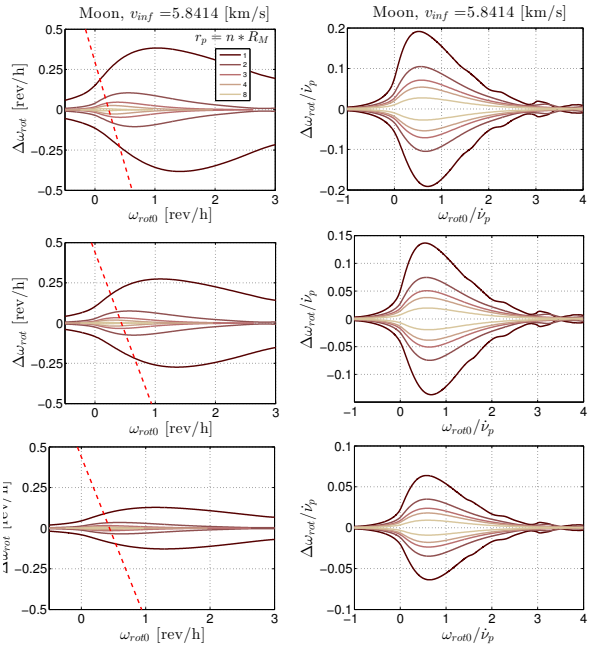

Figure 12: Maximum spin-up and de-spin achievable for a high-velocity Moon swing-by for various shape factors: point-mass dumbbell (top), equal mass contact binary (middle) and ellipsoid with $a = \sqrt{2}b$ (bottom). Right plots have been normalised with the true anomaly rate at pericentre $\dot{\nu}_p$.

pericentre $\dot{\nu}_p$. In the case of the low velocity swing-by, the maximum rotation rate changes scale with this value, and the results can be easily generalised to even higher pericentre radius. For the high velocity swing-by, the maximum normalised values decrease noticeably with the pericentre radius.

Several key conclusions can be drawn from these plots. Consistent with the results for the test cases in section III, no rotation rate variation of practical relevance can be achieved for retrograde asteroids, or for asteroids rotating initially at speeds higher that three times the true anomaly variation at pericentre $\dot{\nu}_p$. The maximum de-spin for low positive (prograde) initial spin rates follows the zero spin rate line for the cases with a high shape factor. This indicates elongated objects can be completely de-spun for a certain range of initial rotation rates. Variations larger than $\dot{\nu}_p$ can be achieved for elongated shapes.

The maximum spin-up occurs for prograde initial rotation rates close to zero, while the maximum de-spin is for asteroids initially rotating at speeds close to $\dot{\nu}_p$. These maxima increase with the elongation of the asteroid shape, and the location of the rotation for maximum spin-up moves away from zero with the swing-by speed, at the same time the initial rotation for maximum de-spin decreases.

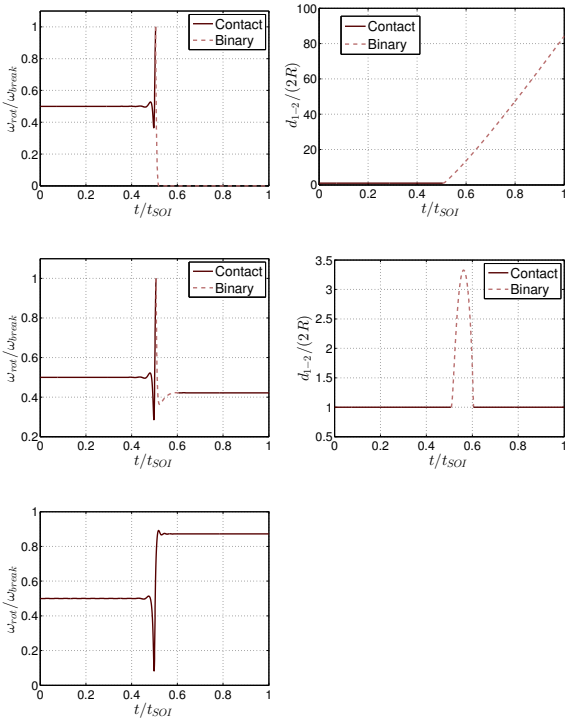

Figure 13: Examples of binary disruption: contact binary break-up, binary pair generation and collapse to contact binary again, and contact binary surviving the swing-by.

IV.II Isolated Lunar Swing-by

For the lunar swing-by case, we consider pericentre radii as low as 1800 km (approximately 63 km above the lunar surface), and up to 8 lunar radii. Figures 11 and 12 show the maximum rotation rate variation for the lunar swing-by cases. Similar conclusions can be drawn, although the perturbations in the high velocity case are much smaller than in the Earth swing-by case for a similar pericentre radius.

Rotation rate changes of the order of the true anomaly rate at pericentre $\dot{\nu}_p$ can still be achieved for the low velocity flyby. However, for the lunar swing-by, a slowly rotating prograde asteroid cannot be completely de-spun: the maximum de-spin does not follow the $y = -x$ line. For the high speed swing-by, the maximum spin-up and de-spin lines appear to be almost symmetric with respect to the horizontal axis, indicating that there is an initial rotation rate for which the largest change can be achieved in either direction depending on the geometric configuration at pericentre. The magnitude of the spin-up and de-spin is much reduced in this case. As a side note, there are small oscillating variations at higher speeds, indicating higher order resonances, but the effects are limited.

Equal mass contact binary break-up

As a final case study, the possibility of break-up of a contact binary was analysed for a low velocity lunar swing-by with a pericentre at two lunar radii. The contact binary is assumed to rotate initially in a prograde direction at half the binary break-up limit.

The results are again very much dependent on the geometry at pericentre passage, and thus the initial conditions. Figure 13 presents three examples of different outcomes. The rotation rates have been scaled with the binary break-up limit, and the time with the total time within the lunar sphere of influence t_{SOI}. In the first case (top figures), the contact binary reaches the break-up limit, and the distance between the binary pair increases due to tidal torques until they effectively break apart from each other. A second case shows a separation into a binary pair that collapses once again into a contact binary during the swing-by. The maximum separation between the two components is larger than 6 times their radius. Finally, there are cases in which the contact binary survives the swing-by without breaking apart at any time, as shown in the bottom plot of Fig.13.

V. CONCLUSIONS AND FURTHER WORK

Swing-bys during the capture phase of an asteroid retrieval mission could be effectively used to de-spin the asteroid, or spin-up and break-up of rubble piles. Several recommendations can be formulated from the previous analysis:

- Assuming a target captured asteroid has been detumbled or de-spun after grappling and bagging (as in the proposal of the Keck study report [3]), and no induced rotation during the capture swing-by phase is desired, introducing a small retrograde rotation for the asteroid (with periods as large as 25 hours) will effectively avoid undesired spin-up effects. This requires very little control, which should be within the capabilities of the retrieval spacecraft if a complete de-spin was performed after bagging. Fast rotators (faster than three times the true anomaly variation at pericentre) are also not affected, but having a controlled fast rotating asteroid is less likely to be feasible or of practical use.

- Assuming a residual prograde rotation of the asteroid at the time of the swing-by that needs to be reduced, small modifications in the time of pericentre passage or in the rotational state would allow a change in the relative attitude of the asteroid at pericentre. Tuning this geometry can completely de-spin the captured asteroid depending on its shape. This is effective for rotation rates slower or of the order of the true anomaly variation at pericentre $\dot{\nu}_p$.

- On the other hand, if spin-up of the captured asteroid is desired for some practical purpose, a similar strategy can be proposed to increase the rotation rate of a slowly rotating asteroid to levels of the order of $\dot{\nu}_p$.

- Induced spin-up can be employed ultimately to break-up a contact binary or rubble pile, for scientific reasons or in the case it would be beneficial for exploitation.

However, this is only a preliminary analysis and the models used need to be improved to confirm the results. A more complex model including the gravitational attraction of the Earth and the Moon should be implemented s appropriate. Most importantly, non-planar models in which the rotation is not constrained to be perpendicular to the orbital plane should also be considered. These will introduce the possibility of tumbling and complex rotation states, but possibly also the opportunity to use tidal toques to de-tumble or stabilize the rotation of an asteroid. Additionally, introducing internal strength and cohesion will significantly affect the outcome of the break-up analysis. As a further step, complex models of asteroid rubble piles, with multiple size and shape mass concentrations held together by self-gravity and cohesion could be devised. Finally, as shown in the previous analysis, the outcomes of a tidal interaction during a swing-by are very sensible to variations in the geometry of the encounter, and small errors may cause large deviations in the final state. Devising control strategies and studying their feasibility is left here for future work.

VI. ACKNOWLEDGEMENTS

The work reported was supported by European Research Council grant 227571 (VISIONSPACE). The attendance to the conference was partly funded by the Institute of Engineering and Technology Travel Award, and the University of Strathclyde's PGR Student Travel Fund.

REFERENCES

[1] Blackburn, E. P., Sabroff, A. E., Bohling, R. F., DeBra, D. B., Dobrotin, B., Fischell, R., Fleig, A. J., Kelly, J., Fosth, D., O'Neill, S., Spenny, C. H., Perkel, H., Roberson, R. E., Scott, E. D. and Tinling, B. [1969]. Spacecraft gravitational torques, *Technical Report NASA SP-8024*, NASA.

[2] Borggräfe, A., Ceriotti, M., Heiligers, J. and McInnes, C. [2012]. Coupled orbit and attitude dynamics of a reconfigurable spacecraft with solar radiation pressure, 63^{rd} *International Astronautical Congress*, IAC-12-C1.9.10, Naples, Italy.

[3] Brophy, J., Culick, F., Friedman, L., Allen, C., Baughman, D., Bellerose, J., Betts, B., Brown, M., Casani, J. and Coradini, M. [2012]. Asteroid retrieval feasibility study, *Technical report*, Keck Institute for Space Studies, Califonia Institute of Technology, JPL.

[4] Chandrasekhar, S. [1963]. The equilibrium and the stability of the Roche ellipsoids, *The Astrophysical Journal* **138**: 1182–1213.

[5] Davidsson, B. J. R. [2001a]. Tidal splitting and rotational breakup of solid spheres, *Icarus* **142**: 525–535.

[6] Davidsson, B. J. R. [2001b]. Tidal splitting and rotational breakup of solid biaxial ellipsoids, *Icarus* **149**: 375–383.

[7] Fang, J. and Margot, J.-L. [2012]. Binary asteroid encounters with terrestrial planets: timescales and effects, *The Astronomical Journal* **143**(25): 1–8.

[8] Farinella, P. and Chauvineau, B. [1993]. On the evolution of binary Earth-approaching asteroids, *Astronomy and Astrophysics* **279**: 251–259.

[9] Richardson, D. C., Bottke, W. F. and Stanley, G. L. [1998]. Tidal distortion and disruption of Earth-crossing asteroids, *Icarus* **134**: 47–76.

[10] Rubincam, D. P. [2000]. Radiative spin-up and spin-down of small asteroids, *Icarus* **148**: 2–11.

[11] Sanchez Cuartielles, J. P., Alessi, E. M., García Yárnoz, D. and McInnes, C. [2013]. Earth resonant gravity assists for asteroid retrieval missions, *64th International Astronatical Congress*, IAC-13,C1,7,8x17808, Beijing, China.

[12] Sánchez, P. and Scheeres, D. J. [2013]. Granular cohesion and fast rotators in the NEA population, *International Conference on Micromechanics of Granular Media. AIP Conference Proceedings*, Vol. 1542, Sidney, Australia, pp. 955–988.

[13] Scheeres, D. J. [2012]. Modelling small body environments, *Orbital Motion in Strongly Perturbed Environments: Applications to Asteroid, Comet and Planetary Satellite Orbiters*, Springer-Verlag Berlin Heidelberg, pp. 23–59.

[14] Scheeres, D. J., Benner, L. A. M., Ostrob, S. J., Rossi, A., Marzari, F. and Washabaugh, P. [2005]. Abrupt alteration of asteroid 2004 MN4's spin state during its 2029 Earth flyby, *Icarus* **178**: 281–283.

[15] Sincarsin, G. B. and Hughes, P. C. [1983]. Gravitational orbit-attitude coupling for very large spacecraft, *Celestial Mechanics* **31**: 143–161.

[16] Strange, N., Landau, D. and Chodas, P. [2014]. Identification of retrievable asteroids with the Tisserand criterion, *SPACE 2014 – AIAA/AAS Astrodynamics Specialist Conference*, AIAA 2014-4458, AIAA/AAS, San Diego, CA, USA.

[17] Toth, J., Veres, P. and Kornos, L. [2011]. Tidal disruption of NEAs - a case of Pribram meteorite, *Monthly Notices of the Royal Astronomical Society* **415**: 1527–1533.

[18] Urrutxua, H., Scheeres, D. J., Bombardelli, C., Gonzalo, J. L. and Pelaez, J. [2014]. What does it take to capture and asteroid? A case study on capturing asteroid 2006 RH120, *24th AAS/AIAA Space Flight Mechanics Meeting*, AAS 14-276, Santa Fe, Mexico.